Hindawi
Advances in Civil Engineering
Volume 2019, Article ID 6571092, 13 pages
https://doi.org/10.1155/2019/6571092

Research Article

Calculation Methods for the Permeability Coefficient of Concrete Face Rockfill Dam with Cracks

Zhongwen Shi[1,2,3] **Zhongru Wu**[1,2,3] **Chongshi Gu**[1,2,3] **Bo Chen**[1,2,3] **Hailong Zhang**[2,4] **Wenzhong Yin**[2,3] **and Bangbin Wu**[2,3]

[1]*State Key Laboratory of Hydrology-Water Resources and Hydraulic Engineering, Hohai University, Nanjing 210098, China*
[2]*College of Water Conservancy and Hydropower Engineering, Hohai University, Nanjing 21009, China*
[3]*National Engineering Research Center of Water Resources Efficient Utilization and Engineering Safety, Hohai University, Nanjing 210098, China*
[4]*Construction and Operation Administration Bureau of Three Gorges Project, China Three Gorges Corporation, Yichang 443000, China*

Correspondence should be addressed to Zhongwen Shi; shizhongwen@hhu.edu.cn and Bo Chen; chenbohhu@126.com

Received 9 January 2019; Accepted 27 February 2019; Published 2 April 2019

Academic Editor: Giovanni Garcea

The permeability coefficient of a concrete slab rockfill dam (CFRD) was calculated in this paper on the basis of the equivalent quasi-continuum model for the percolation of crack-intensive face. This calculation helped simplify the establishment of a finite element model and improve the efficiency of calculating the seepage of dams. Moreover, an inversion algorithm based on particle swarm optimization and support vector machine was proposed and applied. Comparison of the permeability coefficients produced from the two methods showed minimal difference. On this basis, the seepage field of the dam was analyzed. The analysis and field monitoring data reveal that the proposed algorithm is of high application value, which lays a foundation for future studies on the seepage properties of CFRD with cracks.

1. Introduction

Seepage has been a major concern in dam engineering since the face rockfill dam emerged. Design deficiencies in the dam body and antiseepage, damage to the face from squeezing and face cracks, and similar factors will result in leakage and unsteady seepage. Once the face is seriously damaged, its antiseepage function will be weakened; consequently, seepage discharge will increase and flow through the bedding and transition areas, resulting in cracks and collapse of the face [1]. Even worse, a considerably strong seepage discharge will lead to a dam break [2–5]. Regrettable accidents have happened in the construction of concrete slab rockfill dam (CFRD) in China and abroad. For example, during the operation of the San Banxi Dam [6], the external load caused regional damage at the bottom of the face construction joint, such that the vertical joint failed partially, leading to extensive leakage through the dam body as high as 30 L/s. The operation of the dam and safety of a stable seepage were greatly affected. After the Campos Novos CFRD in Brazil [7] stored water, the load from water pressure squeezed and damaged the vertical joint on the water bed, which is as long as 100 m, causing a serious leakage of 1400 L/s. Therefore, data on the permeability coefficients and seepage conditions from field monitoring and simulations must be analyzed to ensure prompt control and normal operation of the CFRD.

Some scholars have used the equivalent continuum method (ECM) and the discrete medium method to solve the problem of fissured flow through CFRD cracks [8, 9, 10]. For instance, Lomize [11] applied a parallel-face seepage experiment to prove the cubic relationship between the seepage flow and unit width of cracks (denoted as the cubic law). They examined the seepage properties on the coarse face and proposed a method for improving the coarse face. The influence of crack size was further investigated by Sagar

and Runchal [12]. Long and Witherspoon [13] performed an in-depth exploration on the influence of crack joints on the seepage tensor. On the basis of the law of hydraulic characteristics in steady seepage through equal-width cracks, Li and Wang [14] developed a seepage model of face joints and cracks, which has been proven feasible in practice. In their establishment of a 3D seepage finite model for the Yangqu Hydropower Station, Zhang and Li [15] analyzed the properties of the 3D steady seepage fields of the dam and its base. Lin and Long [16] analyzed the influence of multiface cracks on the seepage characteristics in the case study of one hydropower CFRD. However, these studies lack relevant monitoring data to prove their results; thus, the feasibility and reasonability of the model proposed in this paper were confirmed by on-spot survey data and simulation.

Cracks on the concrete slab may be caused either by construction and water pressure or by temperature, thereby affecting the permeability coefficient, which is changeable due to the load from water pressure and the dead loads of the cushion, transition layer, and main rockfill. At this time, the permeability coefficient of the concrete slab, cushion, transition layer, and main rockfill can be calculated with monitoring data, which is crucial for improving the analysis on the 3D seepage field and providing an objective assessment of real seepage conditions. At present, numerous scholars have studied the permeability coefficient of earth-rock or core-wall dam on the basis of practical monitoring data. Inverse analysis on the permeability coefficient of earth-rock dam was conducted by Wang et al. [17] using a random forest support vector machine (SVM). An inversion method was proposed by Liu et al. [18] by applying a BP neural network. Liu and Wang [19] introduced a modified genetic algorithm (GA) to invert the coefficient of rock with cracks, and their method is highly effective in regional search and efficient in calculation. In a case study of the Ertan Arch Dam, 3D finite element and GA were used by Cui and Zhu [20] to build an inverse model of an osmotic field. They ascertained the permeability coefficient of the dam base and verified the result. According to the nonlinear mapping of a neural network and with the use of monitoring data, Zhang et al. [21] developed an inversion method to calculate the permeability coefficient. The mutative scale optimization algorithm and general Bayes with finite element were applied by Zheng et al. [22–24], who proposed random inversion in calculating the coefficient. However, inversion study on the permeability coefficient of CFRD remains lacking. Furthermore, qualitative analysis generally dominates the studies on existing earth-rock dams, which considered the total seepage discharge and then the geological parameters and antileakage measures, without incorporating regional seepage discharge. Unlike the abovementioned studies, the current work considers the data of regional seepage and conducts inversion analysis on the permeability coefficient in each part of the CFRD on the basis of particle swarm optimization (PSO) and SVM.

In summary, a method based on PSO and SVM for calculating the permeability coefficient was proposed in this paper from monitoring data of seepage. The algorithm was applied in practice, and the result was compared with that from an equivalent continuum model. The comparison revealed minimal difference between the two methods. The seepage properties were analyzed, and on-spot monitoring data showed that the method proposed is of high application value. Therefore, this study paves the way for further investigations on the seepage properties of CFRD with cracks.

2. Materials and Methods

2.1. Equivalent Quasi-Continuum Medium Model of Seepage through Face Cracks. The problem of seepage through cracks on a single face or through a joint can be regarded as the seepage through cracks on parallel faces. In reality, the length of one crack is considerably longer than its width. Assuming that no water exchange exists along the crack, the mathematical model will be as follows [25].

The governing equation for incompressible fluid is as follows:

$$\begin{cases} \dfrac{\partial v_i}{\partial x_i} = 0, \\ \qquad\qquad (i = x, y, z), \\ \dfrac{\partial v_i}{\partial t} + v_i \dfrac{\partial v_i}{\partial x_i} - f_i + \dfrac{1}{\rho}\dfrac{\partial p}{\partial x_i} - \dfrac{\mu}{\rho}\nabla^2 v_i = 0, \end{cases} \tag{1}$$

where p is the fluid pressure, ρ denotes the fluid density, v_i represents the component of fluid velocity along each coordinate axis, f_i refers to the component of mass force along each coordinate axis, t indicates the time, and μ is the coefficient of dynamic viscosity.

On the basis of Figure 1, the previous equation can be changed into the following equation:

$$\begin{cases} \dfrac{\partial v_x}{\partial x} = 0, \\ \qquad\qquad (i = x, y, z). \\ \dfrac{\partial v_i}{\partial t} + \dfrac{1}{\rho}\dfrac{\partial p}{\partial x} - \dfrac{\mu}{\rho}\dfrac{\partial^2 v_x}{\partial y^2} = 0, \end{cases} \tag{2}$$

Suppose that, at the initial moment, steady flow is present, the initial condition of (2) is as follows:

$$\begin{cases} p|_{t=0} = p_0(x) = p_1^0 + \dfrac{x + (a/2)}{a}\left(p_2^0 - p_1^0\right), \\ \\ v|_{t=0} = v_0(y) = \dfrac{p_2^0 - p_1^0}{8\mu a}\left(4y^2 - b^2\right), \end{cases} \tag{3}$$

where p_1^0 and p_2^0 are the initial fluid pressures on the upstream and downstream cracks, respectively.

Boundary condition satisfies the following equation:

$$\begin{cases} p|_{x=-a/2} = p_1(t), p|_{x=a/2} = p_2(t), \\ v|_{y=-b/2} = v|_{y=b/2} = 0, \end{cases} \tag{4}$$

where $p_1(t)$ and $p_2(t)$ are the seepage pressures on the upstream and downstream cracks, respectively, at t.

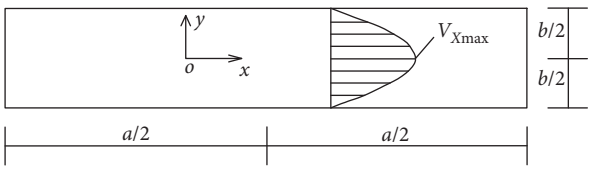

Figure 1: Water flow through equivalent-width cracks.

Through equations (2)–(4), flow velocity and unit discharge of unsteady seepage are calculated as follows:

$$v_x(y,t) = \frac{4y^2 - b^2}{8\mu}\left[\frac{p_2^0 - p_1^0}{a}e^{at} + \frac{\partial p}{\partial x}\left(1 - e^{at}\right)\right],$$
$$q(t) = -\frac{b^3}{12\mu}\left[\frac{p_2^0 - p_1^0}{a}e^{at} + \frac{\partial p}{\partial x}\left(1 - e^{at}\right)\right]. \quad (5)$$

The previous equations describe the process of solving the hydraulic characteristics of unsteady flow. For steady flow, the following equation can be obtained:

$$\frac{\partial^2 v_x}{\partial y^2} = \frac{1}{\mu}\frac{\partial p}{\partial x}. \quad (6)$$

Its boundary condition is the second equation in equation (4). The solvable flow velocity is as follows:

$$v_x(y) = \frac{1}{8\mu}\frac{\partial p}{\partial x}\left(4y^2 - b^2\right). \quad (7)$$

The pressure head on one crack surface is H, the position head is Z, and the hydraulic gradient is J, and the following equation will be obtained:

$$\frac{\partial p}{\partial x} = \frac{\partial[\gamma(H - Z)]}{\partial x} = -\gamma J, \quad (8)$$

where γ denotes the volume weight of water. Equation (7) can be changed into the following equation:

$$v_x(y) = \frac{\gamma}{8\mu}J\left(b^2 - 4y^2\right). \quad (9)$$

Then, the unit discharge of steady flow inside the crack is as follows:

$$q = 2\int_0^{b/2} v_x(y)dy = \frac{\gamma J}{4\mu}\int_0^{b/2}\left(b^2 - 4y^2\right)dy = \frac{b^3\gamma}{12\mu}J, \quad (10)$$

where q is in proportional relation with cubic b, which is the cubic law. The law requires the width of cracks to be equal and the flow inside the cracks to be laminar. Thus, the average velocity can be calculated as follows:

$$V = \frac{q}{b} = \frac{b^2\gamma}{12\mu}J = KJ, \quad (11)$$

where K represents the hydraulic conductivity of the crack.

Several of the existing CFRDs have numerous cracks; thus, this study is crucial. Given the properties of seepage along crack-intensive faces, assuming that numerous cracks are densely distributed is reasonable. That is, most of the cracks traverse the whole crack along the perpendicular direction, such that the seepage mostly penetrates the cracks and the seepage flows are laminar.

With these assumptions, the seepage analysis model can be developed, as shown in Figure 2.

A dense seepage may help create a connected potential surface between the crack-intensive face and cushion, such that piezometer heads downstream are approximately equal, and all piezometer heads upstream are H_0. Therefore, the seepage (J_f) along each crack is approximately equal. The unit discharge from all cracks is as follows:

$$q_f = \sum_{i=1}^{n}\left(K_{f_{ei}}J_f b_{ei}\right) = J_f\sum_{i=1}^{n}\left(K_{f_{ei}}b_{ei}\right),$$
$$b_{ei} = \left(\frac{2b_{0i}^2 b_{ti}^2}{b_{0i} + b_{ti}}\right)^{1/3}, \quad (12)$$

where $K_{f_{ei}}$ is the equivalent permeability coefficient, b_{ei} denotes the equivalent width, and n represents the number of cracks. Seepage through a crack-intensive face can be regarded as a macroscopic quasi-continuous medium seepage, when the seepage slope is J_f. K_{ye} can be used to represent the macroscopic seepage properties. The unit discharge is as follows:

$$q_u = K_{\mathrm{ye}}J_f L, \quad (13)$$

$$K_{\mathrm{ye}} = \frac{\gamma}{12\mu L}\sum_{i=1}^{m} C_i b_{ei}^3, \quad (14)$$

$$C_i = \frac{1}{1 + 8.8\left(\Delta/2b_{ei}\right)^{1.5}}. \quad (15)$$

When Δ (absolute roughness of crack interface), b_{0i} (width of inlet crack), and b_{ti} (width of exit crack) are determined, q_u and K_{ye} can be calculated through equations (13)-(14).

A crack-intensive face is seen as a macroscopic quasi-continuum medium, and its seepage coefficient is regarded as an equivalently uniform seepage coefficient. Despite the tedious and complicated preparation, the calculation efficiency was greatly improved because the distribution features and locations of cracks are irrelevant. Therefore, the face can be divided into meshes and each unit seepage coefficient is K_{ye}, which simplifies the finite model and considerably enhances the calculation efficiency.

2.2. CFRD Seepage Parameter Inversion Based on PSO and SVM

2.2.1. SVM. The SVM was used to develop the model and find a nonlinear mapping [26, 27], which satisfies the regression equation of the vector:

$$f(x,\omega) = (\omega \cdot \Phi(x)) + b, \quad (16)$$

where ω is an n-D weight vector and b represents the threshold value.

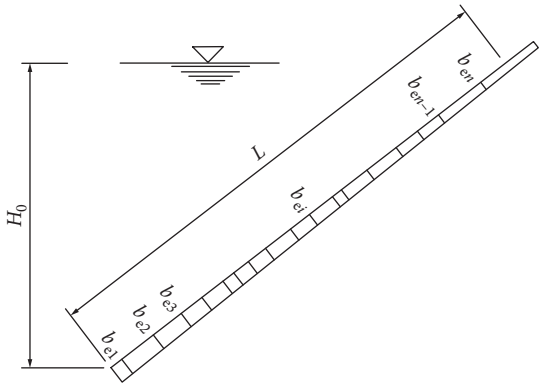

Figure 2: Seepage analysis model.

The insensitivity function ε is defined as an error function, and its constraint condition is as follows:

$$\begin{aligned} y_i - \omega \cdot \Phi(x_i) - b \le \varepsilon, \quad & i = 1, 2, \ldots, k, \\ -y_i + \omega \cdot \Phi(x_i) + b \le \varepsilon, \quad & i = 1, 2, \ldots, k. \end{aligned} \tag{17}$$

The optimum regression hyperplane satisfies that all sample points are close to the hyperplane, and the distance between them are within ε. Figure 3 presents the geometrical importance.

In common regression fitting, the fitting error is considered, which means that the error of some fitting points can exceed ε and the punishment degree of these points must be controlled. Therefore, ξ (positive relaxation coefficient) and γ (punishment factor) were introduced (a large γ indicates a serious punishment). Thus, the fitting was transformed into optimization with constraint conditions:

$$\min \Phi(\omega, b) = \frac{1}{2}\|\omega\|^2 + \gamma \sum_{i=1}^{k} \xi. \tag{18}$$

At this moment, the constraint conditions are as follows:

$$\begin{aligned} y_i - \omega \cdot \Phi(x_i) - b \le \varepsilon + \xi, \quad & i = 1, 2, \ldots, k, \\ -y_i + \omega \cdot \Phi(x_i) + b \le \varepsilon + \xi, \quad & i = 1, 2, \ldots, k. \end{aligned} \tag{19}$$

The solving process for equation (18) is a typical quadratic programming problem. Lagrange $L(\omega, b, \xi, \alpha)$ was introduced to determine the saddle point. Moreover, the nonlinear regression function is as follows:

$$f(x) = \sum_{i=1}^{k} \alpha_i (\Phi(x_i) \cdot \Phi(x)) + b, \tag{20}$$

where α_i denotes the Lagrange multiplier.

Kernel function was used to replace the dot product in the previous equation, which will be changed into the following equation:

$$f(x) = \sum_{i=1}^{k} \alpha_i k(x, x_i) + b. \tag{21}$$

When $\alpha_i = 0$, its corresponding data sample drops out of the summation, so it is a nonsupporting vector.

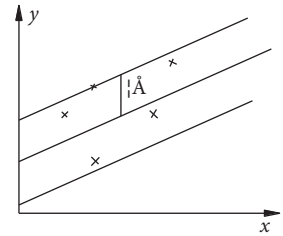

Figure 3: Insensitivity function ε.

Kernel function is a mapping function formed in a high-dimensional space when the input vector goes through a nonlinear transformation, so it determines the nonlinearity of the SVM. That is, different kernel functions require different algorithms. The kernel function, which can precisely reflect the distribution characteristics of samples, will greatly improve the nonlinearity of the SVM.

In this paper, radial-basis kernel function was applied:

$$K(x, x_i) = \exp\left(-\frac{\|x - x_i\|^2}{2\sigma^2}\right), \tag{22}$$

where σ is a parameter of the width of the function, which controls the radial range of the function.

Loss function is used to assess the inconsistent degree between $f(x)$ predicted value and y real value, which is $L(y, f(x))$. The smaller the $L(y, f(x))$, the better the model's robustness. The loss function used in this paper is as follows:

$$e(f(x) - y) = \max(0, |f(x) - y| - \varepsilon). \tag{23}$$

In summary, the SVM is a learning machine for searching a nonlinear mapping function (equation (21)) and transforming the linear mapping function in a high space into the solution of a dual problem. Thus, the complexity of calculation depends only on the number of support vectors in the function.

2.2.2. PSO Algorithm. Particle swarm optimization, proposed by Eberhart and Kennedy in 1995, is a swarm intelligent optimization [28, 29]. This algorithm originates from the observation that the easiest way for birds to find food is to find the food surrounding them. In solving the optimization problem, each particle is a potential optimization and fitness function that can be used to assess the advantages and disadvantages of the particle. The location, velocity, and fitness of one particle keeps updating by tracking individual and group extreme values for an optimization in a solvable space. The PSO includes the following steps.

First, suppose that group $X = (X_1, X_2, \cdots X_n)$ is composed of n particles in a D-dimensional searching space and that particle i is a D-dimensional vector, that is, $X_i = (x_{i1}, x_{i2}, \ldots, x_{iD})^T$, which represents its location in space.

Second, the fitness degree for X_i is calculated through the objective function. Furthermore, the velocity, individual extreme value, and group extreme value of particle i

can be expressed as $V_i = (V_{i1}, V_{i2}, \cdots V_{i\,D})^T$ and $P_g = (P_{g1}, P_{g2}, P_{gD})^T$, respectively, where P_g is the position of the global extremum of the whole particle swarm in the D-dimensional space.

Third, the location and velocity of each particle can be renewed during iteration by tracking the individual and group extreme values, as follows:

$$\begin{aligned} V_{id}^{k+1} &= \omega V_{id}^{k} + c_1 r_1 \left(P_{id}^{k} - X_{id}^{k}\right) + c_2 r_2 \left(P_{gd}^{k} - X_{gd}^{k}\right), \\ X_{id}^{k+1} &= X_{id}^{k} + V_{id}^{k}, \end{aligned} \tag{24}$$

where ω indicates the inertia weight; $d = 1, 2, \ldots, D$, $i = 1, 2, \ldots, n$; k denotes the number of iterations; V_{id} represents the particle velocity; c_1 and c_2 are nonnegative constants, which are acceleration factors; and r_1 and r_2 refer to the random numbers in [0,1].

Finally, the optimum solution is ascertained once the conditions are satisfied.

2.2.3. Inversion of the Permeability Coefficient of CFRD Based on PSO-SVM. With monitoring data on seepage discharge and PSO-SVM, the inversion was performed, as shown in Figure 4. The steps are discussed as follows.

First, the value range of the permeability coefficient was determined on the basis of real engineering. The orthogonal test was adopted to generate the testing program combinations used in the finite element model.

Second, the 3D finite element was used to calculate the testing program in each group. The seepage discharge in each group was computed. Then, the two results will be used as learning samples in the inversion model.

Penalty factor C and kernel parameter σ were selected; the learning samples were used to construct the inversion model between the permeability coefficient and seepage discharge:

$$\begin{aligned} &\mathrm{SVM}(\overline{k}) : R^n \longrightarrow R, \\ &\overline{Q} = SVM(\overline{k}), \\ &\overline{k} = (k_1, k_2, \ldots, k_m), \\ &\overline{Q} = (Q_1, Q_2, \ldots, Q_n), \end{aligned} \tag{25}$$

where $\overline{k}$ is the permeability coefficient vector to be inversed, m denotes the number of permeability coefficients, and $\overline{Q}$ represents the vector of seepage discharge.

Fourth, on the basis of the inversion model, the least error between the calculated and measured values of seepage discharge was used as the objective function; then, the best combination of the permeability coefficient was determined through PSO.

The objective function is as follows:

$$\min S = \frac{1}{n}\sum_{i=1}^{n} \left(Q_i - Q_i^*\right)^2. \tag{26}$$

The constraint condition is as follows:

$$\underline{k_j} \le k_j \le \overline{k_j}, \quad j = 1, 2, \ldots, m, \tag{27}$$

where $\underline{k_j}$ and $\overline{k_j}$ are the minimum and the maximum of permeability coefficient and m denotes the number of permeability coefficients.

3. Case Study

The equivalent continuum model was used to calculate the equivalent permeability coefficient of one face of CFRD; the inversion method based on PS-SBVM was adopted in the inversion of the coefficient. The seepage fields identified from the two methods were compared; monitoring data verified the feasibility of the model and inversion method.

3.1. Engineering Introduction. The highest body of one CFRD is 120.0 m, and the elevation of its top is 760.00 m; the top extends as long as 259.8 m from east to west and the face is as thick as $t = 0.3 + 0.00347H$(m), which changes linearly from up to down, that is, 0.3 m at the top and 0.7 m at the bottom. The upstream slope is 1 : 1.4, whereas the downstream slope is 1 : 1.35. On February 6, 2004, the faces were checked, and 180 cracks were found. In 2012, a total of 206 cracks were found.

In all studies on CFRDs, no regional seepage discharge has been measured [30]. Almost all of them proceed from the monitoring of total seepage discharge and then qualitative analysis with geological parameters and antiseepage measures. However, in this paper, the regional seepage discharge was measured first, and then, an intercepting ditch was set at the foot of two bank slopes in accordance with the landform and locations of surrounding buildings to block the seepage discharge from two banks, such that the seepage can flow into the measuring weir set downstream. The intercepting ditch goes all the way down from the upstream face at an average gradient of 1%. The major measuring weir is set at the dam toe, which divides the seepage discharge into abutment, face, and base seepages. On the basis of the landform and structure, the seepage discharge at the two measuring weirs, namely, W1 and W2, is mainly the abutment seepage. The retaining wall set where the plant meets the dam foot leads the seepage to a certain location, where W3 was set. The seepage discharge at W3 is face, base, and W1 and W2 seepages. Figures 5 and 6 show the distribution of measuring weirs and the measurement line of seepage, respectively. The seepage discharge at W1 and W2 is relatively small, indicating that the antiseepage at the two banks is effective.

3.2. Calculation of Equivalent Permeability Coefficient. Figure 7 presents the onsite inspection of regional cracks, whereas Figure 8 displays all cracks. Considering the limited space, Table 1 only lists 26 cracks on the largest fracture surface relative to the distribution height (z_i), equivalent width (b_{ei}), and relative roughness of the dam base ($\Delta/2b_{ei}$). After calculation, the equivalent uniform permeability coefficient is 3.17×10^{-10} m/s.

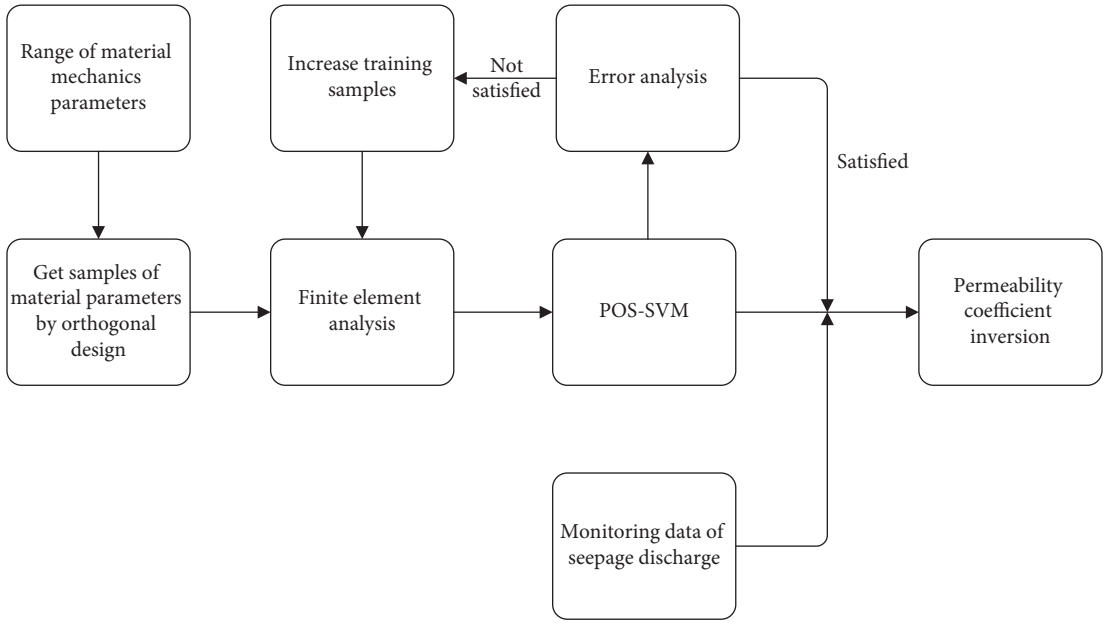

Figure 4: Flow of the permeability coefficient inversion.

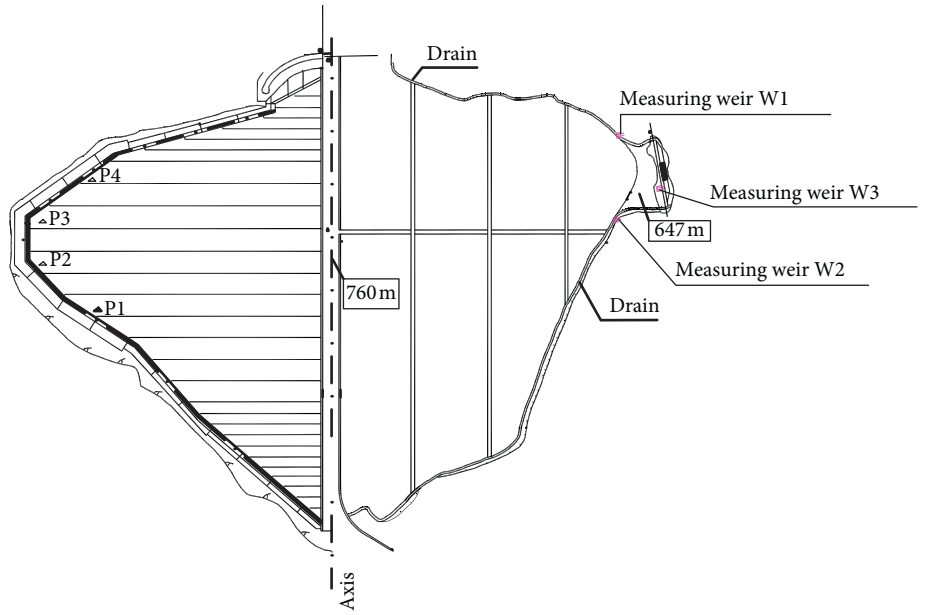

Figure 5: Distribution of measuring weirs.

3.3. Finite Element Simulation Calculation

3.3.1. 3D Finite Element Model. Figure 9 illustrates the 3D finite model of CFRD and the dam body mesh. The coordinate is a user-defined system, where the direction from top to bottom along the *X*-axis is positive, the direction from right to left along the *Y*-axis is positive, and the direction from bottom to top along the *Z*-axis is positive. This model applies to the area from 1.5 times of the dam height across the two banks and the equivalent of the dam height from the base rock, dam front, and dam back. The main boundary that may influence the seepage field was considered in the model. Face region, bedding region, transition layer, main rockfill region, and secondary rockfill region were simulated in high precision. The curtain, peripheral joint, toe slab, and rock body on both banks were accurately divided into meshes. A total of 53,027 units and 56,593 nodes were present in the model. Hexahedron-shaped units with eight nodes were mainly used, whereas a few triprism shaped units were also utilized for support.

3.3.2. Boundary Conditions. In the model, the following boundary conditions were mainly considered:

Bedrock boundary: the basic depth of area analyzed was set at 120 m. Undrained boundary was adopted as the intercepting boundary in this analysis.

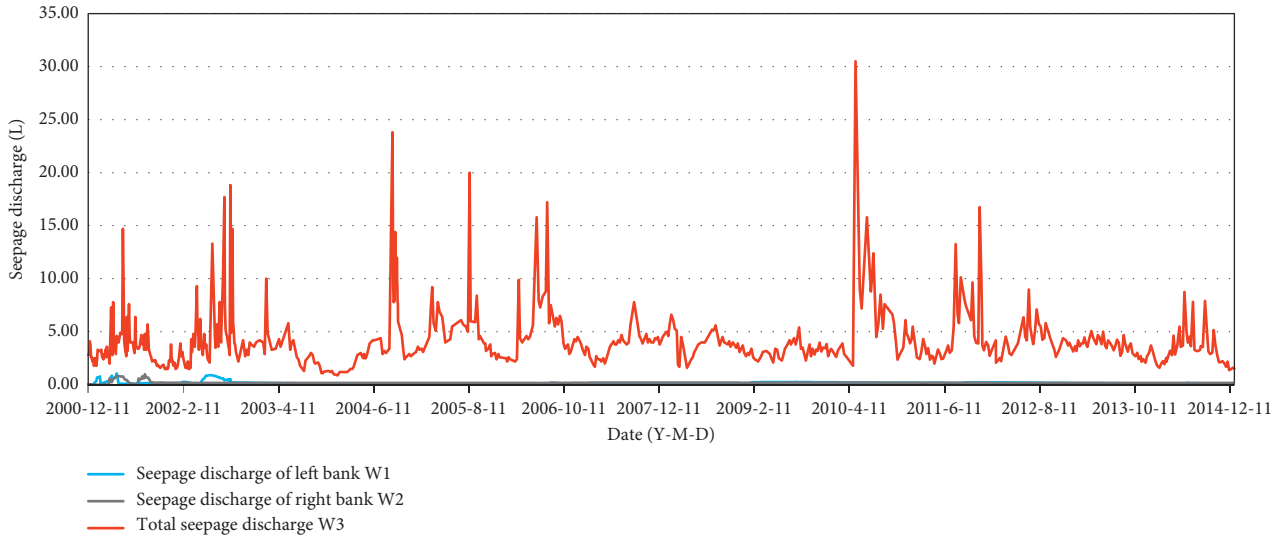

Figure 6: Monitoring data of seepage discharge.

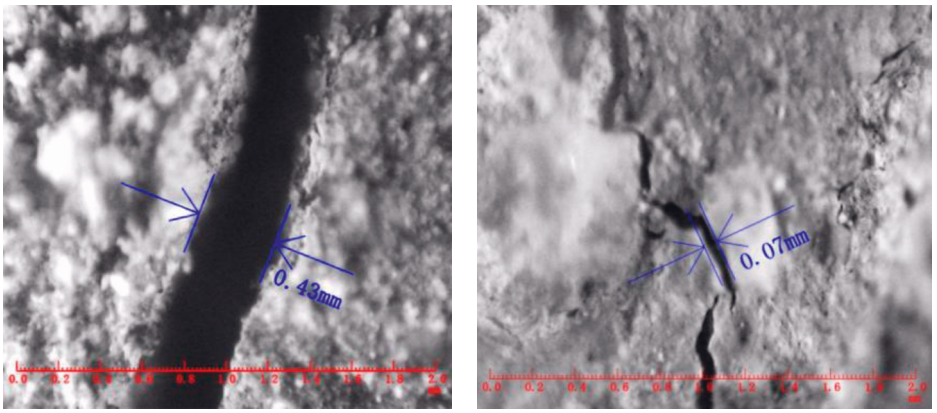

(a) (b)

Figure 7: Onsite inspection of regional cracks.

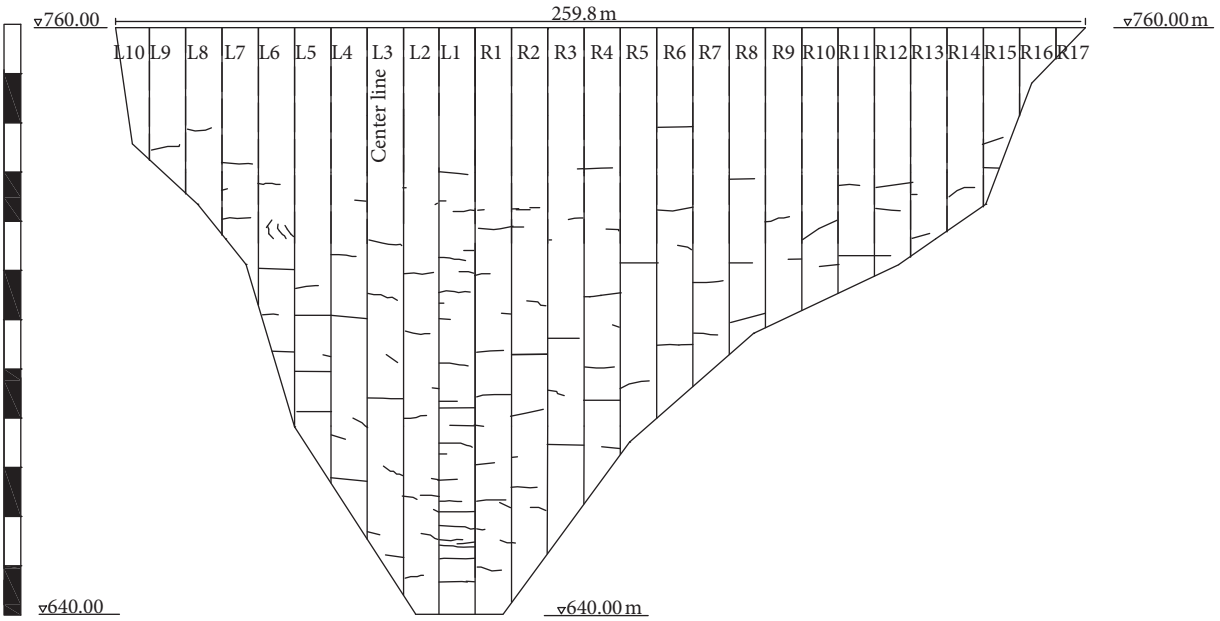

Figure 8: Distribution of all cracks.

Table 1: Parameters of cracks.

i	z_i (m)	b_{ei} (mm)	$\Delta/2b_{ei}$	i	z_i (m)	b_{ei} (mm)	$\Delta/2b_{ei}$
1	7.98	0.05	0.30	14	48.89	0.31	0.31
2	8.51	0.22	0.34	15	53.01	0.37	0.24
3	12.89	0.17	0.29	16	56.64	0.41	0.43
4	13.15	0.16	0.34	17	56.81	0.29	0.31
5	14.47	0.12	0.21	18	77.42	0.28	0.34
6	17.96	0.24	0.27	19	77.53	0.07	0.29
7	26.39	0.33	0.23	20	86.77	0.40	0.28
8	29.90	0.37	0.27	21	86.96	0.35	0.31
9	30.62	0.48	0.24	22	87.42	0.28	0.18
10	34.21	0.23	0.46	23	90.34	0.38	0.26
11	34.60	0.46	0.33	24	90.85	0.26	0.29
12	40.55	0.43	0.21	25	95.11	0.16	0.44
13	43.93	0.05	0.30	26	106.75	0.13	0.27

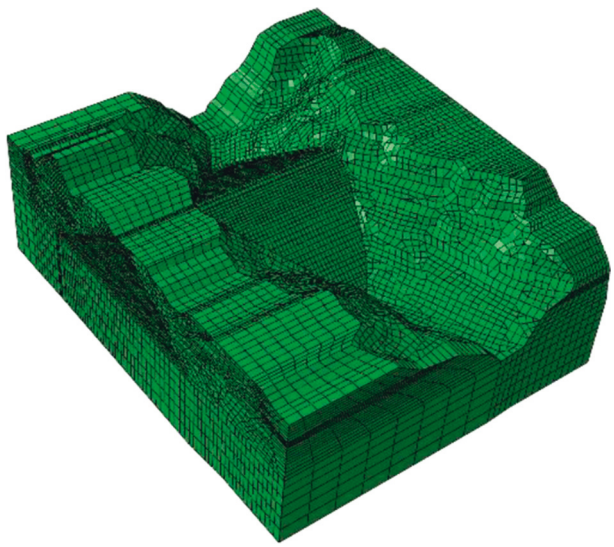

Figure 9: 3D finite element model of CFRD.

Upstream and downstream boundaries of the dam area: monitoring data on the geological conditions of the dam and the underground water distribution were used as references to assess the seepage situation to fill the underground water in the dam bed. For the comparisons of seepage discharges, the flow of underground water along the water flow at the bed is believed to be negligible. Therefore, the flow exchange at the boundary is zero, which indicates undrained boundary.

Known boundary of the water level: to avoid the influence of rainfall, the water level without rainfall for a long time was used upstream. The bed below the water level upstream and downstream was set as the known boundary of constant head.

Potential overflow boundary: seepage may happen at the dam body above the water level at the upstream bed and at the rock surface on both banks. Thus, in the calculations, seepage was regarded as potential overflow boundary, and the final iteration result was used to see whether seepage occurred.

Bank bounadary: as the level of underground water at both banks is higher than the water head at the bed, the overall seepage flows to the bed as supplement seepage. Hence, the boundary conditions on both banks were considered water head boundaries.

3.4. Permeability Coefficient Inversion. Upstream water level and rainfall are two major factors influencing seepage discharge, and Figure 10 shows the monitoring process. In selecting data for inversion, using the data gathered when the water level is steady with minimal rainfall is highly recommended so that the inversion results will be closer to reality. The seepage discharge data in this paper were collected during a steady period (October 1–30, 2012). Figure 11 presents the water level and rainfall hydrograph. Average seepage discharge observed was used in the inversion. The average level of 736.95 m was used as the water head boundary in the finite element algorithm.

Table 2 displays the value ranges of the permeability coefficient of concrete slab, cushion, transition layer, and major rockfill. On the basis of the range of permeability coefficient to be inverted, five levels of each factor were used; 25 calculation conditions were created through orthogonal design. Tables 3 and 4 present the values of the factor levels and the calculation conditions.

Initial parameters were set as 200 times for the group iteration and 20 for the number of groups. The permeability coefficient of each material was calculated through the inversion algorithm, which is shown in Table 5. Figure 12 illustrates the hydrograph of the particle swarm iteration. It can be seen from Table 5 that the inversion result of the permeability coefficient is 2.52×10^{-10} m/s, which is 20% smaller than the result of the equivalent uniform method.

To verify the reasonability of the inversion results, prior analysis was conducted on seven sets of seepage discharge data observed when the water level was steady with minimal rainfall (no rainfall in at least 15 days). The calculated value was revealed to be close to the measured value. Table 6 displays the calculation results.

3.5. Seepage Analysis. On the basis of the designed data and seepage parameters from inversion, the seepage properties in cases of normal water level, designed flood level, and check flood level were calculated. Table 7 lists the parameters.

Figures 13–15 present the typical section contour lines of the calculation results in three conditions. The saturation line inside the face goes down sharply before a slow drop, and the whole line is low in the middle while high on both ends, indicating that the antiseepage system composed by face and curtain is relatively effective. Thus, measuring the regional seepage discharge at the measuring weir is reasonable. Inversion calculation can qualitatively reflect how the crack emerged, which is helpful for managers to know the condition of seepage for normal dam operation.

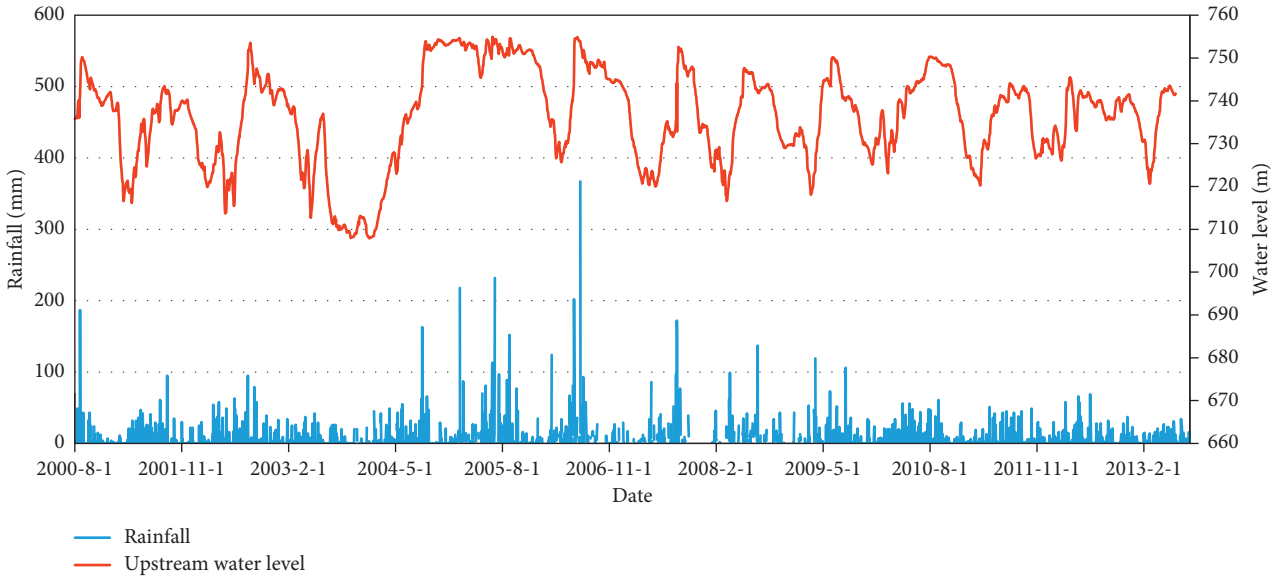

Figure 10: Monitoring data of upstream water level and rainfall.

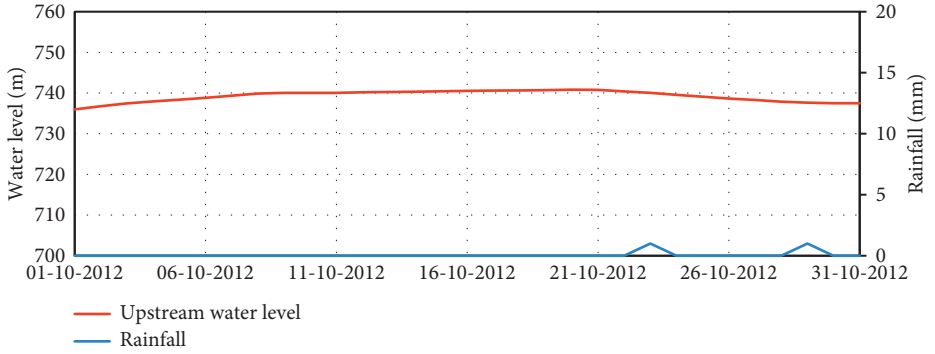

Figure 11: Water level and rainfall during the steady period (2012-10-1 to 2012-10-31).

Table 2: Permeability coefficients to be inverted.

Material	Permeability coefficient (m/s)
Concrete slab	1×10^{-11}~1×10^{-9}
Cushion	1×10^{-6}~1×10^{-5}
Transition layer	1×10^{-4}~1×10^{-3}
Major rockfill	0.0001~0.01

Table 3: Level of each factor.

i	Permeability coefficient (m/s)			
	Concrete slab	Cushion	Transition layer	Major rockfill
1	1×10^{-11}	1×10^{-6}	1×10^{-4}	0.0001
2	6×10^{-11}	3.5×10^{-6}	3.5×10^{-4}	0.0005
3	1×10^{-10}	6×10^{-6}	6×10^{-4}	0.001
4	5.5×10^{-9}	8.5×10^{-6}	8.5×10^{-4}	0.005
5	1×10^{-9}	1×10^{-5}	1×10^{-3}	0.01

4. Discussion

Despite there are 206 cracks on the concrete slab, as shown in Figure 8, the monitoring values of seepage discharge are low (less than 4 L/s, during 2012-10-1 to 2012-10-31). The reasons for that are (1) among all the cracks, only part of the cracks are penetrating and (2) the cushion and transition layer behind the concrete slab still can work well for antiseepage.

There is 20% difference between the results from the two methods, and it is hard to say which method is more accurate, but when there is only monitoring data of seepage discharge, the PSO-SVM inversion method could be more appropriate; conversely, if there are no monitoring data of seepage discharge, the equivalent quasi-continuum model should be adopted. When using the equivalent quasi-continuum model, parameters of all cracks should be measured, which usually takes a lot material resources and time. Most hydropower stations only carry out cracks detection once every few years. Conversely, the monitoring data of seepage discharge usually can be got easily by measuring weirs. So, the PSO-SVM inversion method can be suitable and justified for most cases.

5. Conclusions

Various shapes of cracks may appear on the face of the CFRD during construction or storage due to its thickness

Table 4: Calculation conditions and results of the finite element algorithm.

Test	Permeability coefficient (m/s)				Calculated seepage discharge (L/s)
	Concrete slab	Cushion	Transition layer	Major rockfill	
1	1×10^{-11}	1×10^{-6}	1×10^{-4}	0.0001	2.63
2	1×10^{-11}	3.5×10^{-6}	3.5×10^{-4}	0.0005	2.91
3	1×10^{-11}	6×10^{-6}	6×10^{-4}	0.001	2.95
4	1×10^{-11}	8.5×10^{-6}	8.5×10^{-4}	0.005	3.01
5	1×10^{-11}	1×10^{-5}	1×10^{-3}	0.01	3.04
6	6×10^{-11}	1×10^{-6}	3.5×10^{-4}	0.001	2.92
7	6×10^{-11}	3.5×10^{-6}	6×10^{-4}	0.005	3.01
8	6×10^{-11}	6×10^{-6}	8.5×10^{-4}	0.01	3.05
9	6×10^{-11}	8.5×10^{-6}	1×10^{-3}	0.0001	2.68
10	6×10^{-11}	1×10^{-5}	1×10^{-4}	0.0005	2.93
11	1×10^{-11}	1×10^{-6}	6×10^{-4}	0.01	3.02
12	1×10^{-10}	3.5×10^{-6}	8.5×10^{-4}	0.0001	2.68
13	1×10^{-10}	6×10^{-6}	1×10^{-3}	0.0005	2.94
14	1×10^{-10}	8.5×10^{-6}	1×10^{-4}	0.001	2.98
15	1×10^{-10}	1×10^{-5}	3.5×10^{-4}	0.005	3.04
16	5.5×10^{-10}	1×10^{-6}	8.5×10^{-4}	0.0005	2.91
17	5.5×10^{-10}	3.5×10^{-6}	1×10^{-3}	0.001	2.98
18	5.5×10^{-10}	6×10^{-6}	1×10^{-4}	0.005	3.05
19	5.5×10^{-10}	8.5×10^{-6}	3.5×10^{-4}	0.01	3.08
20	5.5×10^{-10}	1×10^{-5}	6×10^{-4}	0.0001	2.7
21	1×10^{-9}	1×10^{-6}	1×10^{-3}	0.005	3.01
22	1×10^{-9}	3.5×10^{-6}	1×10^{-4}	0.01	3.07
23	1×10^{-9}	6×10^{-6}	3.5×10^{-4}	0.0001	2.70
24	1×10^{-9}	8.5×10^{-6}	6×10^{-4}	0.0005	2.96
25	1×10^{-9}	1×10^{-5}	8.5×10^{-4}	0.001	3.00

Table 5: Inversion results of the permeability coefficient (m/s).

Concrete slab	Cushion	Transition layer	Major rockfill
2.52×10^{-10}	5.11×10^{-6}	5.57×10^{-4}	4.34×10^{-2}

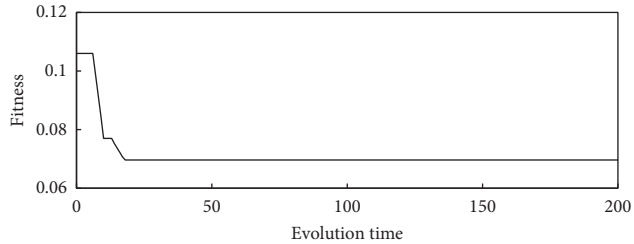

Figure 12: Hydrograph of particle swarm iteration.

Table 6: Comparisons between calculated and monitoring values.

Date	Upstream water (m)	Calculated seepage discharge (L/s)	Monitoring seepage discharge (L/s)	Calculated data-monitoring data/monitoring data (%)
2004-12-19	753.09	3.23	3.1	4.02
2008-12-20	738.76	3.46	3.7	6.49
2009-11-6	740.63	3.1	2.86	4.98
2009-12-7	737.55	3.03	3.15	3.81
2010-11-6	749.95	3.67	3.98	7.79
2011-12-24	745.56	3.48	3.7	5.95
2012-10-15	738.18	3.04	3.32	8.43

Table 7: Dam body materials and permeability coefficient k of rock (m/s).

Material	Concrete slab	Cushion	Transition layer	Major rockfill	Bedrock	Toe slab	Peripheral joints	Curtain	Rock	Parapet wall
k	2.85×10^{-10}	5.11×10^{-6}	5.57×10^{-4}	4.34×10^{-2}	1.5×10^{-7}	1×10^{-10}	1×10^{-10}	5×10^{-8}	1.5×10^{-7}	1×10^{-10}

In the analysis, the calculation conditions are normal water level (755.00 m), designed flood level (756.2 m), and check flood level (759.1 m).

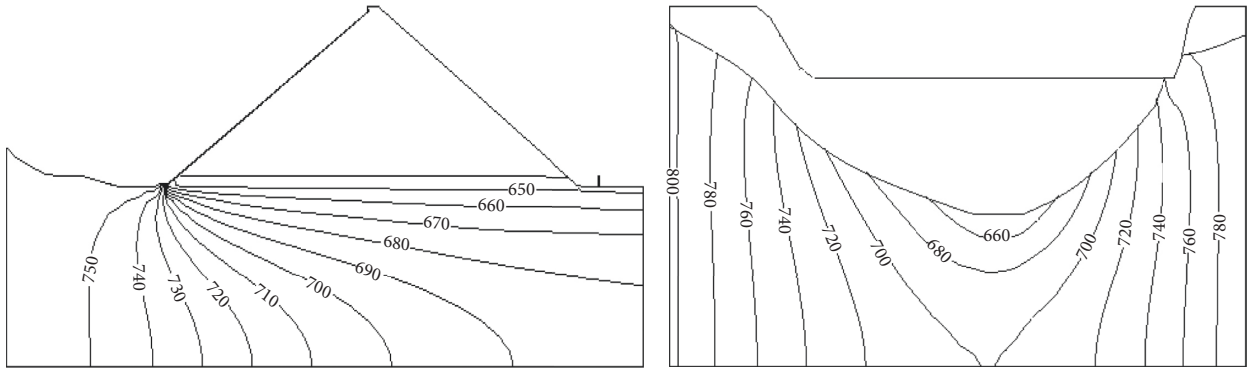

(a) (b)

Figure 13: Typical section contour line of seepage pressure in case of the normal water level (m): (a) contour line of seepage pressure of river bed section and (b) contour line of seepage pressure of dam axis section.

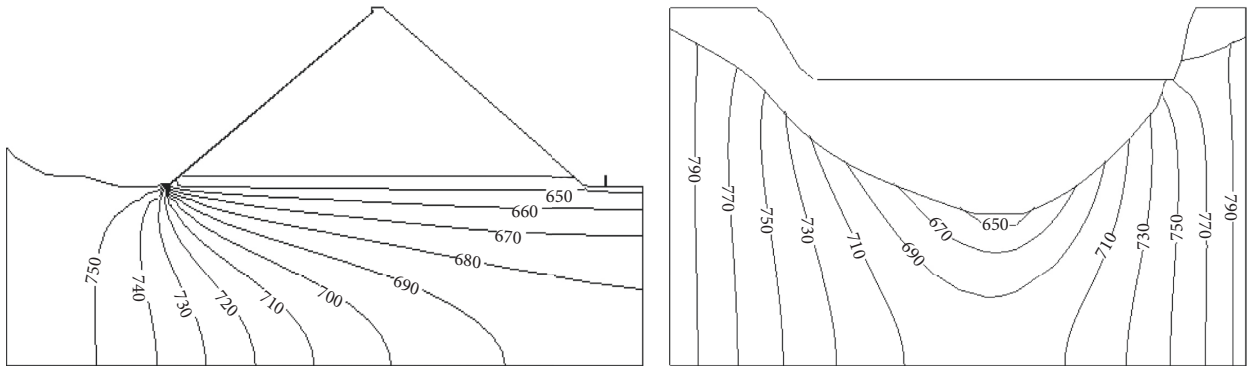

(a) (b)

Figure 14: Typical section contour line of seepage pressure in case of the designed flood level (m): (a) contour line of seepage pressure of river bed section and (b) contour line of seepage pressure of dam axis section.

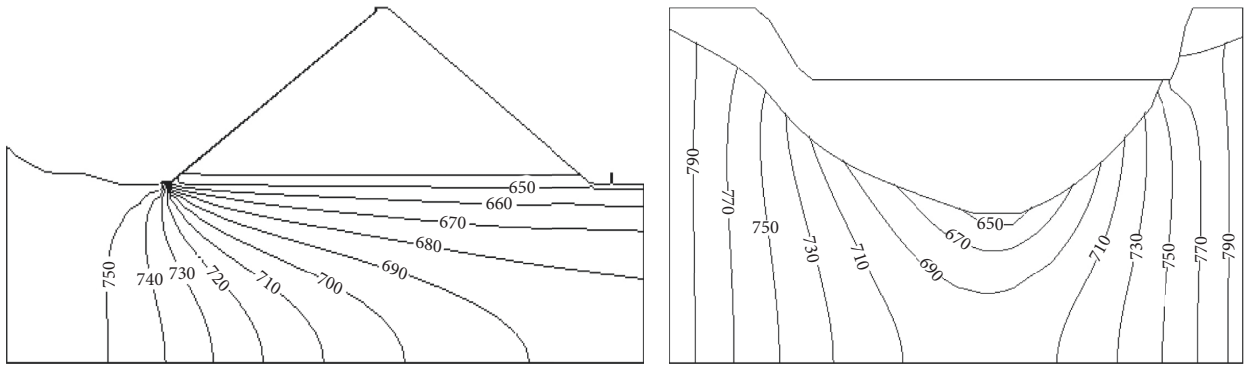

(a) (b)

Figure 15: Typical section contour line of seepage pressure in case of the check flood level (m): (a) contour line of seepage pressure of river bed section and (b) contour line of seepage pressure of dam axis section.

and stiffness difference relative to the cushion, which is harmful to its antiseepage system. Considering the important role of concrete slabs in the antiseepage system of the CFRD, the quality of these faces must be under strict control to reduce the damage caused by seepage from cracks, and checking the cracks regularly is necessary.

The permeability coefficient of the CFRD was calculated in the equivalent continuum medium model, which simplifies the construction of the finite element model and improves the calculation efficiency. The inversion algorithm based on PSO-SVM proved satisfactory in inverting the permeability coefficient with monitoring data. With the coefficients from the two methods, seepage discharge was identified, which was relatively close to the monitoring value, indicating that the two methods are feasible and applicable. This study lays the necessary foundation for further studies on the seepage features of CFRD cracks.

Conversely, measuring the regional seepage discharge can help identify the accurate discharge at each part, thereby safeguarding a secure operation of the monitor, narrowing down the searching range for accidents in an emergency, avoiding blindness, and facilitating the testing of the antiseepage effect on both banks, the waterstop effect of peripheral joints, and the working conditions of concrete slabs.

Data Availability

The data on cracks used to support the findings of this study are available from the corresponding author upon request. The other data used to support the findings of this study are included within the article.

Conflicts of Interest

The authors declare no conflicts of interest.

Acknowledgments

This study was funded by the National Key R&D Program of China (2016YFC0401601, 2017YFC0804607, and 2018YFC0407104), National Natural Science Foundation of China (Grant nos. 51739003, 51479054, 51779086, 51579086, 51379068, 51579083, 51579085, and 51609074), Project Funded by the Priority Academic Program Development of Jiangsu Higher Education Institutions (YS11001), Jiangsu Natural Science Foundation (Grant no. BK20160872), Special Project Funded by National Key Laboratory (20165042112), Key R&D Program of Guangxi (AB17195074), and Central University Basic Research Project (2017B11114 and 2018B25514).

References

[1] NIU, "Security of high concrete slab rockfill dam consideration and conclusion," *Journal of Hydroelectric Engineering*, vol. 36, no. 1, pp. 104–111, 2017.

[2] Yang, Tan, and Zhou, "Discussion on several issues of concrete slab rockfill dam," *Yangtze River*, vol. 47, no. 14, pp. 56–59, 2016.

[3] E. Li, Z. Fu, S. Chen et al., "Numerical simulation of hydraulic fracturing in earth and rockfill dam using extended finite element method," *Advances in Civil Engineering*, vol. 2018, Article ID 1782686, 8 pages, 2018.

[4] M. Rashidi and H. Rasouli, "Initial hypotheses for modeling and numerical analysis of rockfill and earth dams and their effects on the results of the analysis," *Advances in Civil Engineering*, vol. 2018, Article ID 3974675, 7 pages, 2018.

[5] Y. Wu, Q. Zou, Z. Tan et al., "Progress of safety monitoring technology for concrete face rockfill dams in China," *Hydropower and pumped storage*, vol. 3, no. 1, pp. 24–31, 2017.

[6] L. Zhu and Du, "Analysis on stress and strain before and after the face-slab damage of Sanbanxi dam," *Dam and Safety*, vol. 6, pp. 46–48, 2009.

[7] G. Xu, "Experience and lessons from Campos Novos CFRD in Brazil," *Journal of China Institute of Water Resources and Hydropower Research*, vol. 3, pp. 233–240, 2007.

[8] L. Altarejos-García, I. Escuder-Bueno, and A. Morales-Torres, "Advances on the failure analysis of the dam-foundation interface of concrete dams," *Materials*, vol. 8, no. 12, pp. 8255–8278, 2015.

[9] B. Stojanovic, N. M. Milivojevic, and D. Antonijevic, "A self-tuning system for dam behavior modeling based on evolving artificial neural networks," *Advances in Engineering Software*, vol. 97, pp. 85–95, 2016.

[10] C. Liu, Z. Shen, L. Gan et al., "A hybrid finite volume and extended finite element method for hydraulic fracturing with cohesive crack propagation in quasi-brittle materials," *Materials*, vol. 11, no. 10, p. 1921, 2018.

[11] G. M. Lomize, *Flow in Fractured Rocks*, Gesenergoizdat, Moscow, Russia, 1951.

[12] B. Sagar and A. Runchal, "Permeability of fractured rock: effect of fracture size and data uncertainties," *Water Resources Research*, vol. 18, no. 2, pp. 266–274, 1982.

[13] J. C. S. Long and P. A. Witherspoon, "The relationship of the degree of interconnection to permeability in fracture networks," *Journal of Geophysical Research*, vol. 90, no. B4, pp. 3087–3098, 1985.

[14] Li and Wang, "Study on seepage calculation model of concrete slab rockfill dam faceplate," *Chinese journal of applied mechanics*, vol. 27, no. 1, pp. 145–150, 2010.

[15] Zhang and Li, "Seepage behavior analysis of concrete slab rockfill dam," *Journal of Water Resources and Architectural Engineering*, vol. 14, no. 1, pp. 223–226, 2016.

[16] Lin and Long, "The analysis for the impact of the cracks in the panel of Rockfill Dams on seepage characteristics," *Jilin Water Resources*, vol. 10, pp. 1–5, 2012.

[17] Wang, Song, and Yao, "Study on inversion calculation of seepage coefficient of earth rock dam," *Low Temperature Architecture Technology*, vol. 39, no. 3, pp. 87–89, 2017.

[18] Liu, Zhou, and Xun, "Inversion analysis of seepage field based on BP neural network," *China Water Transport*, vol. 14, no. 10, pp. 113–116, 2014.

[19] Liu and Wang, "Improved genetic algorithm and its application in inversion of seepage parameters," *Geotechnical Mechanics*, vol. 2, pp. 237–241, 2003.

[20] Cui and Zhu, "Back analysis of seepage field in dam foundation of two beach high arch dam," *Geotechnical Mechanics*, vol. 30, no. 10, pp. 3194–3199, 2009.

[21] Zhang, Wang, and Wu, "Inverse analysis of dam seepage coefficient based on artificial neural network," *Hydropower and Energy Science*, vol. 4, pp. 4–7, 2001.

[22] Zheng and Wang, "Application of generalized Bayes method in stochastic inversion of permeability coefficient of fractured

rock mass," *Journal of Water Conservancy*, vol. 4, pp. 419–425, 2008.

[23] Chen, Teng, and Wang, "Inversion method of permeability coefficient parameters based on GA-SVR," *Hydrogeology and engineering geology*, vol. 38, no. 2, pp. 14–18, 2011.

[24] B. Chen, C. Gu, T. Bao, B. Wu, and H. Su, "Failure analysis method of concrete arch dam based on elastic strain energy criterion," *Engineering Failure Analysis*, vol. 60, pp. 363–373, 2016.

[25] S.-y. Li, Z. Y.-l. Li, and X.-f. Zhang, "A seepage computational model of face slab cracks based on equi-width joint constant flow," *Advances in Engineering Software*, vol. 41, no. 7-8, pp. 1000–1004, 2010.

[26] N. Barakat and A. P. Bradley, "Rule extraction from support vector machines: a review," *Neurocomputing*, vol. 74, no. 1–3, pp. 178–190, 2010.

[27] D. Basak, S. Pal, and D. C. Patranabis, "Support vector regression," *Neural Inf Process Lett Rev*, vol. 11, pp. 203–224, 2007.

[28] V. Vapnik, *The Nature of Statistical Learning Theory*, Springer-Verlag, New York, NY, USA, 1995.

[29] V. Fathi and G. Ali Montazer, "An improvement in RBF learning algorithm based on PSO for real time applications," *Neurocomputing*, vol. 111, no. 2, pp. 169–176, 2016.

[30] Zhang, Gu, and Wu, "Seepage monitoring model of earth rock dam based on lag effect," *Journal of Water Conservancy*, vol. 2, pp. 85–89, 2001.